SEMARAK ILMU PUBLISHING

Journal of Advanced Research in Fluid Mechanics and Thermal Sciences

Journal homepage:
https://semarakilmu.com.my/journals/index.php/fluid_mechanics_thermal_sciences/index
ISSN: 2289-7879

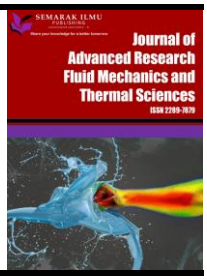

Hydrodynamics Analysis of Mixing Process in Fermenter

Novia Novia[1,*], Jerry Hardian[1], Richard Sepriyadi Osman[1], Getari Kasmiarti[2], Hasanudin Hasanudin[3], Hermansyah Hermansyah[3]

[1] Department of Chemical Engineering, Faculty of Engineering, Universitas Sriwijaya, Indralaya 30662, Sumatera Selatan, Indonesia
[2] Doctoral Program of Environmental Science, Graduate Program Universitas Sriwijaya, Jalan Padang Selasa No.524, Bukit Besar, Palembang 30139, South Sumatra, Indonesia
[3] Department of Chemical Science, Faculty of Mathematics and Natural Sciences, Universitas Sriwijaya, Indralaya 30662, Sumatera Selatan, Indonesia

ARTICLE INFO

Article history:
Received 28 May 2023
Received in revised form 13 August 2023
Accepted 23 August 2023
Available online 9 September 2023

Keywords:
CFD; hydrodynamics; fermenter; mixing

ABSTRACT

The perfect mixing process ensures the ideal substrate conditions for microorganisms to live to produce ethanol in the fermenter. The critical factors that affect the mixing process are the agitation speed, baffle configuration, and the impeller type. The Computational Fluid Dynamics (CFD) software can make the study of fermenter hydrodynamics more convenient due to the cost savings of expensive apparatus and less time-consuming. This study aimed to examine the hydrodynamic characteristics of a fermenter using the ANSYS FLUENT 2021 R1 software and its validation. The hydrodynamics of the mixing process in the dual-pitched blade impeller bioethanol fermenter in agitation speeds of 200 to 1000 RPM and the effect of baffles were observed by simulation and experimentally. The realizable k-epsilon turbulence model and the Eulerian volume of fluid mixture multiphase model were used in this CFD simulation. The simulation results were relatively close to the experimental with similar flow patterns and low mixing time error, which is 7.9% on average. The results show that the higher the agitation speed, the higher the torque, power, and shear stress. The increasing agitation speed caused the lower mixing time. A faster mixing time was obtained in the fermenter with no baffle configuration.

1. Introduction

Mass transfer, heat or temperature transfer, dilution rate for continuous systems, mechanisms for monitoring microbial conditions, process optimization, factors hydrodynamics, process safety, and bioreactor economy are essential factors that must be considered in designing or operating a bioreactor [1]. Mixing in bioreactors is necessary for homogenization within the reactor volume and achieving adequate transport rates while also being a significant cost factor [2]. Diverse bioreactor designs and impeller types have been offered to optimize mass transfer. Examples of reactor designs include single and multiple impellers, semi-partition bioreactors, single-use bioreactors, and membrane bioreactors [3-8]. In addition to the various bioreactor designs, numerous impeller kinds

* *Corresponding author.*
E-mail address: novia@ft.unsri.ac.id

https://doi.org/10.37934/arfmts.109.1.7190

were recommended, using Rushton turbine and counter rotation U-shape impellers [9,10]. Commonly used types of impellers are Rushton turbine and axial or radial. Despite this development, the hydrodynamic characteristics of bioreactors continue to be measured, such as power consumption and interphase mass transfer. Experimental procedures and functional relationships for designing and sizing bioreactors are frequently replaced by Computational Fluid Dynamics (CFD) with models of varying complexity [11].

Cell growing, nutrient application, heat loss, bubble volume, and product conversion requires hydrodynamics and fluid dynamics in a bioreactor [12,13]. Therefore, mixing is the essential factor that has a crucial impact on the microorganism to improve the utilization of medium components [10]. Agitation in the fermenter ensures that mass and heat transfer occurs evenly at each point. The agitation system uses forces against the fluid that produce circulatory movements, distributions, and interactions between biological components. Mixing efficiency is determined by the impeller's rate, flow, and mixing pattern [14]. If the stirring speed is too high, it can cause a vortex or vortex to form in the middle of the bioreactor [15]. The yeast is evenly distributed in the fermenter due to optimal mixing, resulting in maximum interaction between the yeast and sugar (mainly glucose), which optimizes the fermentations [16]. Therefore, it is necessary to dilute glucose with water to create conditions suitable for yeast. It is needed to investigate water content's effect on glucose's rheological characteristics to investigate the optimal conditions of fermentations.

A multiphase model is used in handling systems with more than one phase or the same phase that do not mix. One of the existing multiphase models is the Euler-Euler approach. In this approach, the fluid and dispersed phases are assumed to be continuous, interpenetrating continua. This concept introduces the volume fraction into the calculation [17]. The volume fraction of each continuous phase (continua) will occupy the same volume at a point, so the sum of fractions will always be one. Phases are assumed separately and calculated one by one separately. Turbulence is a fluid phenomenon that occurs during high-speed gradients so that there is a disturbance in the flow domain. The Navier-Stokes equation of unsteady conditions predicts the speed and area of pressure in the laminar regime. K-ε realizable turbulence modeling is one of three turbulence models offered in Fluent ANSYS. The first model is the standard k-ε, and the second is RNG k-ε, a derivative of the standard model using group theory normalization statistical techniques. The realizable k-ε model differs from the standard k-ε model. The k-ε realizable model has an alternative formulation to turbulent viscosity. The dissipation rate equation is modified from derivatives to transport average fluctuations in vorticity. This model satisfies the mathematical problems of the Reynold voltage, consistent with the physicality of the turbulent flow. Models of this type can predict the flow in which rotational motion is better than standard models and RNG k-ε [18,19].

CFD has been acknowledged as a valuable tool for numerical simulations of engineering problems, both design, and operation. CFD simulates the inaccessible areas of reactors and uncontrollable design and operation variables. CFD analyses have been widely utilized in bioprocesses over the past two decades and can practically affect operations. This CFD code comprises three main components: the pre-processor, solver, and post-processor [14]. CFDs have the advantage compared to other optimization methods, namely low costs, reduced workload, and short design period time [15]. CFD employs computational methods to simulate fluid flows based on Navier-Stokes equations utilizing fluid flow properties and geometry [20]. In addition, computational domains aid in virtual prototyping prediction. It is helpful in situations where experiments are bordered and gives benefits for testing different variables such as fluid flow pattern, production strategy improvement, and simulated design's financial effectiveness [10].

Because the bioreactors typically operate on the optimal states, CFD techniques promise to predict adequate flow typicals for existing or new designs [12]. Simulations of fluid dynamics reduce

design time, improve operating conditions' accuracy, are less costly, and can be used as a guide for large-scale industrial [21]. CFD modeling can investigate mixing flow regimes, velocity profiles, operating conditions, design variables, geometry, pressure, and heat distribution [10]. Oo *et al.,* [22] found that the flow characteristics and spacing affect the heat transfer enhancement. Using Stream Analysis Model, Alsadig *et al.,* [23] simulated the Baffled Shell and Tube Heat Exchanger. While the CFD model has been verified with experimental data, a substantial amount of information can be extracted at a portion of the experiment's cost [24].

Numerous CFD techniques have been used to study reactors with baffles, which is not the situation for unbaffled reactors. A few uses of CFD in unbaffled reactors are accessible in the works [24-26]. Some are offered to the laminar regime unbaffled reactors [24]. Others also deal with turbulent regimes [26]. Glover *et al.,* [27] studied the CFD simulation of vortex creation in unbaffled reactors. Rotondi *et al.,* [28] used tests and CFD modeling to examine their reactor to improve microorganism cells. By experimentally and CFD simulation, Davoody *et al.,* [26] found the scaling creation in baffled and unbaffled reactors below the turbulent regime. A transient RANS model was conducted to model baffled and unbaffled reactors. They discovered the scaling creation in unbaffled more than baffled reactors. Li *et al.,* [29] used the CFD simulation with a Reynolds stress and the Volume of Fluid (VOF) model to examine a reactor with Pitched Blade Turbine. However, none of the prior works has been dedicated to distinguishing between baffled and unbaffled fermenters. This study investigated the glucose–water mixing behavior within baffled and unbaffled fermenters using a simple visualization method and a computational study revealing turbulence phenomena via CFD.

2. Methodology

Experiments were conducted to determine the shear stress of glucose–water mixture and glucose–water mixing behavior in unbaffled and baffled fermenter tanks. Then, computational modeling revealed the fluid dynamics of mixing glucose and water within turbulent flows. The ANSYS Fluent 2021 R1 performed the modeling.

2.1 Experimental Procedure

The experiments consisted of two distinct phases. First, the shear stress of the glucose–water mixture was characterized. The second step involved using a visualization technique to investigate the mixing behavior. The coloring / decoloring method carried out the experimental validation method, which refers to Conti *et al.,* [30]. First, 20 mL iodine solution 0.188 M was diluted with 7.5 mL iodine 0.5 M in 12.5 mL of demineralized water. Then, 15 mL sodium thiosulfate 0.5 N was diluted with 5 mL of demineralized water to make 20 mL sodium thiosulfate solution 0.375 N. Next, the fermenter was filled with 1.85 L glucose solution and was added with 20 mL iodine solution 0.188 M. Furthermore, the color of the solution became brown. Finally, 20 mL sodium thiosulfate solution 0.375 N was added to the glucose solution colored with iodine, and the mechanical stirring process. The mixing process was observed and recorded using a digital camera. Mixing time was obtained when the mixture was subjected to total decoloring (the reaction reached equilibrium). Photos obtained through recording with a digital camera were then processed and analyzed. The quantitative results of mixing time and visual qualitative of mixing dynamics were then compared with the post-processing results of the CFD mixing tank simulation that have been obtained.

2.2 CFD Modelling and Numerical Procedure

One baffled and one unbaffled laboratory-sized fermenter were investigated. Both vessels had a diameter of T, equivalent to 0.20 meters, and were placed at a height of H, equal to T. In both vessels, a four-blade Rushton turbine was installed. It was filled in the fermenters at a space C (clearance) from the fermenter bottom equivalent to T/3 and had a diameter D equivalent to T/2. Figure 1 depicts the fermenter as well as all of the impeller components. The geometry of the fermenter is made with the Ansys Space Claim, while the meshing is done using the Ansys Fluent Meshing. The geometry used was a three-dimensional cylindrical fermenter tank with two stirrers 4-blade axial turbine. The zone of the fermenter tank consists of three fluid zones: the stationary zone, the top rotary zone (upper impeller), and the bottom rotary zone (lower impeller). The computational grid detail of the fermenter is shown in Figure 2. An appropriate cover was applied in the fermenters to prevent the center vortex characteristic of unbaffled tanks. The open cap and the existence of a vortex would necessitate a unique action of the free surface, obscuring the turbulence flow's effect and making it more difficult to compare the flow patterns. Various impeller speeds were studied.

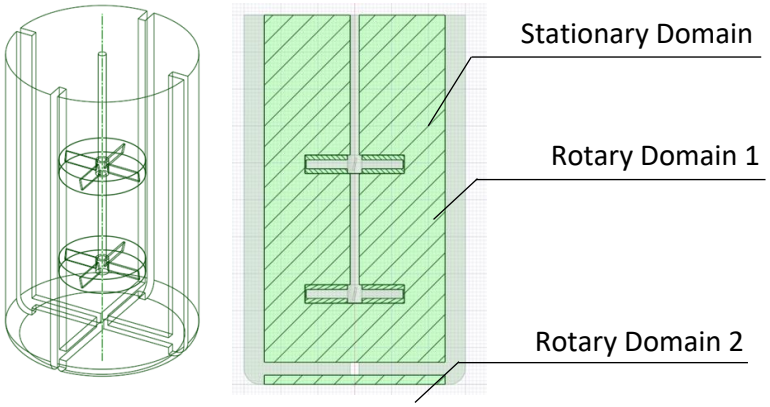

Fig. 1. The geometry of the baffled fermenter

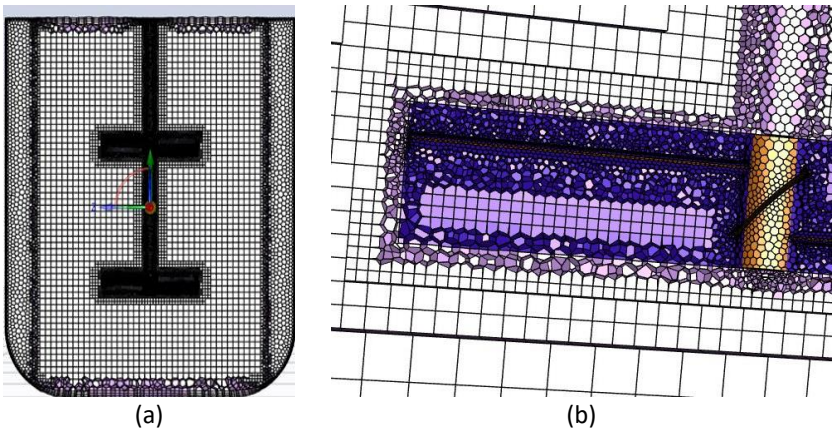

(a) (b)

Fig. 2. Meshing of fermenter: (a) The computational domain (b) grid generation

All simulations were done by solving the mass and momentum conservations, omitted for brevity [17]. Given the objective of this study, CFD techniques were conducted to predict the flow pattern in both fermenters at different impeller speeds. The realizable k-ε turbulence model computed Reynolds stresses. It remains the predominant turbulence model, particularly in the industrial sector

[24]. The eddy viscosity was calculated from k and ε using the Prandtl-Kolmogorov formulation. All simulations were carried out by using the Ansys®FLUENT 2021 software.

These domain boundaries comprise the fermenter bottom, top lid, side wall, baffles, impeller blades, disk, and shaft. These are regarded as walls with non-slip perimeter circumstances. It was adopted that the shaft and baffles had zero thickness. Therefore, baffles were included as part of the tank's perimeter with baffles. All simulations were conducted from the impeller's frame of reference for the tank without a baffle. Therefore, counter-spinning speed was imposed as a boundary condition on the fermenter side, bottom, and top-lid wall in this instance. In contrast, non-slip conditions were imposed on the impeller boundaries. On the momentum equations, body forces were included to take into account the centrifugal and Coriolis properties [24].

2.3 Power Measurement

The power in the bioreactor can be expressed into a dimensionless number called a power number. The power number value can be calculated by connecting several aspects of the fermenter, such as power, fluid density, impeller speed, and impeller diameter. In addition to being expressed in electrical or other energy that drives the impeller, the power number value can also be expressed in torque. Power can be converted into the form of torque generated when impeller rotation occurs [31].

2.4 Torque

Each torque value on each impeller speed was acquired from the simulation with CFD. The torque value is directly proportional to the power of the impeller; the higher power of the impeller, the higher of energy consumption. Therefore, the equation can calculate the impeller power in each fermenter tank mixing condition [32]. The average values of torque, total torque, and total power during the mixing process are presented in Table 1.

$$P = \frac{\pi M N_{rpm}}{30} \tag{1}$$

Table 1
Average values of torque, total torque, and total power at various variables

Tank Configuration	Stirring speed (rpm)	Average Torque (Nm)		Total Torque (Nm)	Total Power (W)
		Bottom Impeller	Top Impeller		
Baffle	200	-	-	-	-
	400	-0.0044	-0.0047	-0.0091	0.3819
	600	-0.0095	-0.0102	-0.0197	1.2370
	800	-0.0168	-0.0176	-0.0344	2.8827
	1000	-0.0266	-0.0267	-0.0533	5.5822
Unbaffle	200	-0.0022	-0.0018	-0.0041	0.0851
	400	-0.0058	-0.0049	-0.0107	0.4479
	600	-0.0111	-0.0100	-0.0211	1.3248
	800	-0.0179	-0.0170	-0.0348	2.9175
	1000	-0.0259	-0.0240	-0.0499	5.2272

2.5 Shear Stress

Shear stress is related to the cell resistance of microorganisms in the stirring process caused by turbulence. According to Nienow [33], if the cell size is smaller than the Kolmogorov length scale (le), the cell will not be damaged due to turbulence. The Kolmogorov length scale is a critical value when a cell is damaged due to turbulence, it can be calculated using Eq. (2). The shear stress calculation was carried out using Eq. (3) [21]. Density, dynamic viscosity, average turbulence energy dissipation rate and kinematic viscosity were used to determine the Kolmogorov length scale and shear stress obtained from the CFD simulation. The calculation of the average shear stress was carried out on four types of zones, namely Rotary Domain 1 (upper impeller), Rotary Domain 2 (lower impeller), Stationary Domain (the rest of the entire zone), and the overall average of the zone. The calculation results can be seen in Table 2.

$$l_e = \left(\frac{\mu^3}{\rho^3 \varepsilon}\right)^{\frac{1}{4}} \tag{2}$$

$$\tau_t = \frac{5}{2}\mu\sqrt{\frac{\varepsilon}{6\nu}}, jika\ d_{cell} < l_e \tag{3}$$

$$\tau_d = \rho(\varepsilon d_{cell})^{\frac{2}{3}}, jika\ d_{cell} > l_e \tag{4}$$

Table 2
Kolmogorov length scale value and average shear stress in various conditions and zones

Fermenter Configuration	Stirring speed (rpm)	Fermenter Zone	l_e(m) × 10^{-6}	τ_t (Pa)
Baffle	400	Rotary Domain 1	491.8833	46.9814
		Rotary Domain 2	431.7514	60.9793
		Stationary Domain	1,655.6229	4.1469
		Overall Average	1,144.0641	8.6846
	600	Rotary Domain 1	408.8489	52.7221
		Rotary Domain 2	371.9772	63.6921
		Stationary Domain	1,239.1748	5.7392
		Overall Average	939.1246	9.9924
	800	Rotary Domain 1	334.4625	63.9010
		Rotary Domain 2	294.1662	82.6070
		Stationary Domain	963.8466	7.6946
		Overall Average	745.0447	12.8777
	1000	Rotary Domain 1	265.0896	73.0239
		Rotary Domain 2	227.3966	99.2390
		Stationary Domain	712.2673	10.1150
		Overall Average	569.5044	15.8218
Unbaffle	200	Rotary Domain 1	933.8451	35.1287
		Rotary Domain 2	752.3373	54.1236
		Stationary Domain	2,238.8448	6.1117
		Overall Average	1,869.3122	8.7669
	400	Rotary Domain 1	594.7198	48.0793
		Rotary Domain 2	527.7804	61.0487
		Stationary Domain	1,574.7714	6.8572
		Overall Average	1,289.8962	10.2205
	600	Rotary Domain 1	482.9167	49.3293
		Rotary Domain 2	375.0447	81.7868

	Stationary Domain	1,428.7990	5.6352
	Overall Average	1,026.3083	10.9218
800	Rotary Domain 1	466.6175	66.7938
	Rotary Domain 2	375.1085	103.3580
	Stationary Domain	1,281.3178	8.8582
	Overall Average	957.2261	15.8719
1000	Rotary Domain 1	282.5382	109.8982
	Rotary Domain 2	283.6798	109.0154
	Stationary Domain	889.3063	11.0928
	Overall Average	683.7142	18.7670

2.6 Mixing Time

Mixing time is measured by calculating the duration required to achieve a homogeneous phase in the mixing process. On CFD simulation, glucose concentration at 4 points in the fermenter tank is observed against changes in time. The location of these four measuring points consists of the bottom, middle, left, and right points of the inside of the fermenter can be seen in Figure 3.

Fig. 3. Observation points of glucose concentration in the fermenter

2.7 Governing Equations

The multiphase hydrodynamics were simulated using the volume of Fluid (VOF) method. The conservation equations in ANSYS FLUENT 2021 R1 CFD software were discretized using the finite volume method.

2.7.1 Continuity equation

The interfaces between the phases can be tracked by solving a continuity equation for the volume fraction of one (or more) of the phases. This equation for the q^{th} phase has the following form [17]:

$$\frac{1}{\rho_q}\left[\frac{\partial}{\partial t}\left(\alpha_q\rho_q\right)+\nabla.\left(\alpha_q\rho_q\vec{v}_q\right)=S_{\alpha_q}+\sum_{p=1}^{n}\left(\dot{m}_{pq-}\dot{m}_{qp}\right)\right] \quad (5)$$

2.7.2 Momentum equation

Across the domain, a singular momentum equation is solved, and the resulting velocity field is shared among the phases. The momentum equation is dependent on the volume fractions of all phases via their properties ρ and μ [17]:

$$\frac{\partial}{\partial t}(\rho\vec{v}) + \nabla.\left(\rho\overrightarrow{v\vec{v}}\right) = -\nabla p + \nabla.[\mu(\nabla\vec{v} + \vec{v}^{T})] + \rho\vec{g} + \vec{F} \quad (6)$$

2.7.3 Energy equation

The energy equation, which is shared by all phases, is displayed below [17]:

$$\frac{\partial}{\partial t}(\rho E) + \nabla.\left(\vec{v}(\rho E + \rho)\right) = \nabla.\left(k_{eff}\nabla\mathrm{T} - \sum_q \sum_j h_{j,q}\vec{J}_{j,q} + \left(\bar{\bar{\tau}}_{eff}.\vec{v}\right)\right) + S_h \quad (7)$$

2.7.4 The rheology properties of the fluid

The CFD model was developed based on the rheological properties shown in Table 3.

Table 3
The rheology properties of the fluid

Property	Glucose	Water
Density (kg/m^3)	1420	997
Specific heat (J/kg.K)	1244	1996
Thermal conductivity (W/m.K)	0.32564	0.598
Viscosity (Pa.s)	0.00139	0.0091

3. Results and Discussion

3.1 Rheological Properties

Data on the average shear stress of all Rotary Domain 2 zones and zones under various conditions are visualized in a graph seen in Figure 4. It can be seen from Figure 6 that the shear stress value in tanks without baffles is greater than the value of tanks with baffles. The higher impeller speed increased the shear stress value. The highest shear stress value was obtained, 18.7670 Pa, in the unbaffled tank at a speed of 1000 rpm. Shear stress values measured in this study are higher than the shear stress limit of 2.5 Pa, identified by Odeleye *et al.,* [34]. The limit value of shear stress for *Saccharomyces cerevisiae* is between 1292 Pa and 2770 Pa [35]. For speeds of 200-1000 RPM, the shear stress of the mixing process is difficult to damage the cell because of its small value compared to the threshold the cell can withstand.

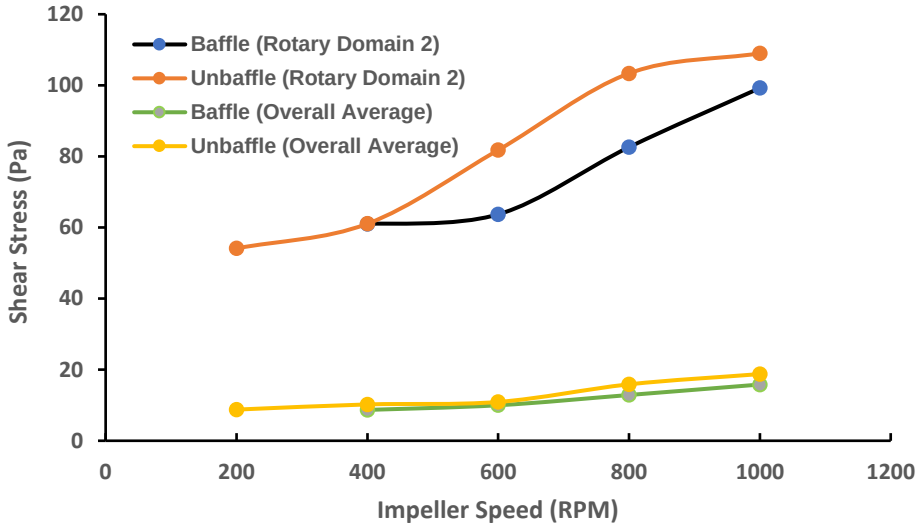

Fig. 4. Effect of impeller speed on shear stress

3.2 Effects of Fermenter Configurations on Hydrodynamics

In this section, the effect of fermenter configurations on the vortex and flow patterns was investigated in depth. The homogeneous flows can be assessed in the alterations of water volume fraction in plane-XY of unbaffled and baffle fermenter with 600 RPM, as depicted in Figure 5 and Figure 6, respectively. From these two pictures, the alterations in the contours of the water volume fraction the whole time expose that the mixing happens from the beginning of stirring until homogeneity is achieved. The alteration in contour can be used to illustrate the observed turbulence in the fermenter. There is no dead zone in the final stirring state; therefore, the mixing degrees are 0.9984 (unbaffled fermenter) and 0.9937 (baffle fermenter). Figure 5 and Figure 6 depict the contour plots of the vertical cross-section of the water volume fraction between the experiment and simulation at various times. This diagram illustrates relative heterogeneity in the vessel at different times for an impeller speed of 600 RPM. A vortex will develop without baffles, and the flow will be controlled by tangential flow in the fermenter [36]. The free surface vertices are described in Figure 5, and glucose is unseen for clearness. A long vortex spreads, beginning the liquid superficial to the impeller in the unbaffled fermenter. Due to the flow field's insufficient development, the free surface vortex is not evident.

Consequently, more glucose is diffused, and the height of their suspension increases. At 15 s and 60 s, a noticeable vortex was visible under the impeller. Upon reaching a steady state at 180 s, the height of the glucose suspension reduces, and the vortex becomes a little smaller. The free surface vortex and glucose circulation growth in experimental and CFD simulations are relatively similar throughout the mixing.

As shown in Figure 5, the water volume fraction is more remarkable at 260 s mixing time. Higher glucose density and sufficient driving power produced by the Rushton impeller at 600 rpm are responsible for the higher water volume fraction at 260 s mixing time. The inadequate flow motion has been restored by raising the mixing time to 300 s; consequently, the red region at the tank's surface has shrunk. For a mixing time of less than 260 s, there is still some heterogeneity at the tank's bottom. With an increase in mixing time to 300 s, an entirely homogenous condition was achieved because of an increase in turbulent kinetic energy and the re-circulation rate caused by the impeller [34]. Because the secondary phase is traced at the bottom-fermenter prior to the mixing process, the impeller's pumping rate is insufficient for a mixing time of fewer than 260 s. Lower impeller off-

bottom clearance could contribute to a greater circulation rate and a more uniform flow inside the fermenter at lower impeller speeds [37].

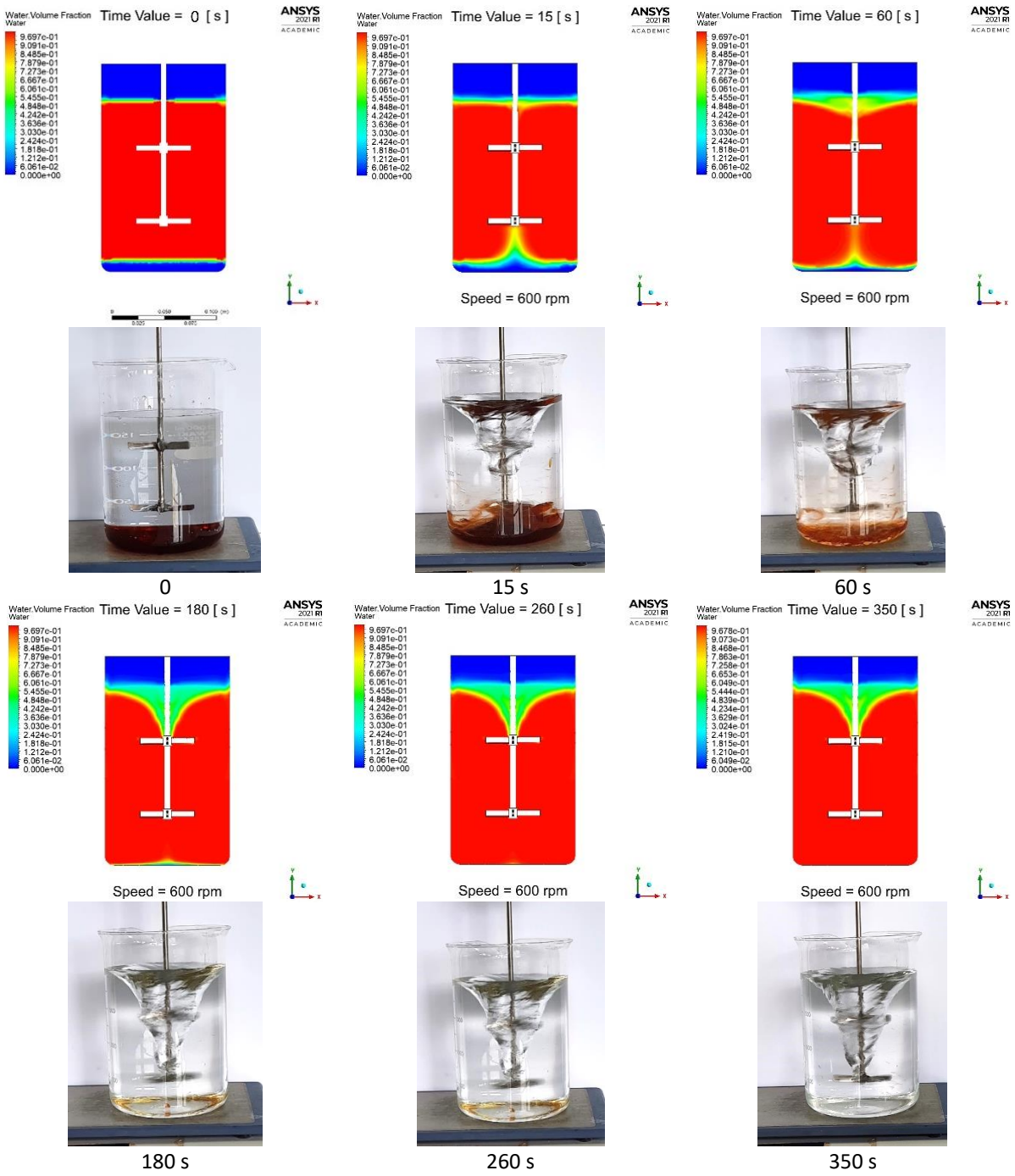

Fig. 5. Snapshots of simulated concentration contours in a 2 L unbaffled fermenter (Top). Snapshots of red dye mixing in the 2 L unbaffled fermenter with 600 RPM (Bottom). Red and blue indicate high and low water volume fractions, respectively

Figure 6 illustrates the higher water volume fraction at 705 s mixing time. Higher glucose density and sufficient pumping power produced by the Rushton impeller at 600 rpm are responsible for the higher water volume fraction at 705 s mixing time. The inadequate flow dynamic has been restored by enhancing the mixing time to 880 s; consequently, the red region at the tank's surface has shrunk. For mixing time less than 705 s, there is still some heterogeneity at the tank's bottom. With an

increase in mixing time to 880 s, an entirely homogenous condition was achieved because of an increase in turbulent kinetic energy and an increase in the re-circulation rate induced by the impeller [34]. As depicted in Figure 6, the recommended procedure for the glucose–water mixing process was based on visual observations and comprised three distinct zones. In the first zone, the interface height increases marginally during the brief period when the impeller has just begun to rotate. As the impeller rotates, glucose in direct contact is drawn toward the impeller in a negative-axial direction. This phenomenon occurs because the impeller has lost its pumping capacity due to the high viscosity of glucose [16]. Initially, the impeller transfers the energy only reaches the glucose at the blade bend. The length of the mixing process causes the impact of impeller rotation to increase until it achieves the interface region, causing water to be pulled in, diffuse the interface border, and then travel in the way of the flow pattern produced by the impeller rotation. As the area where the pulled-up glucose is typically located is then filled by water, the glucose requires a new location to occupy, increasing interface height. In addition, the VOF model can simulate the hydrodynamic alterations and glucose distribution behaviors detected in the experiment. The simulation results agree well with the experimental data.

Zone two phenomena resemble zone one phenomenon. The impeller's capacity to disperse water in the glucose-rich area, affected by the mixture's rheology, particularly viscosity, causes the interface height to change slowly over a long time. Changes in the fluid mixture's properties surrounding the impeller impacted its pumping capacity. At specific locations on the interface's surface, turbulence conditions cause fluid to enter zone three. The majority of the mixing stages happen in zone three. Other authors reported the same investigation to predict the mixing property [16,30].

Figure 7 depicts an unbaffled fermenter's velocity vector at the XZ plane—strong relationships between flow patterns and the free surface vortex. There were three parts of circulation loops visible in the fermenter. The two upper loops comprise a fluid stream departing the propeller till the fermenter's rim, flowing upward and down to the impeller side, which is influenced by the free surface vertices. In addition, a small loop is formed at the bottom vessel to wall section due to the quick flow diversions. According to studies, the velocities inside caused loops are lower than in bulk flow. As a result, these loops' glucose has slower speeds and suspend later than the other area of the glucose in the fermenter. Thus, achieving the fluidization speed for all glucose particles and finishing the off-bottom mixture will require significant energy [36].

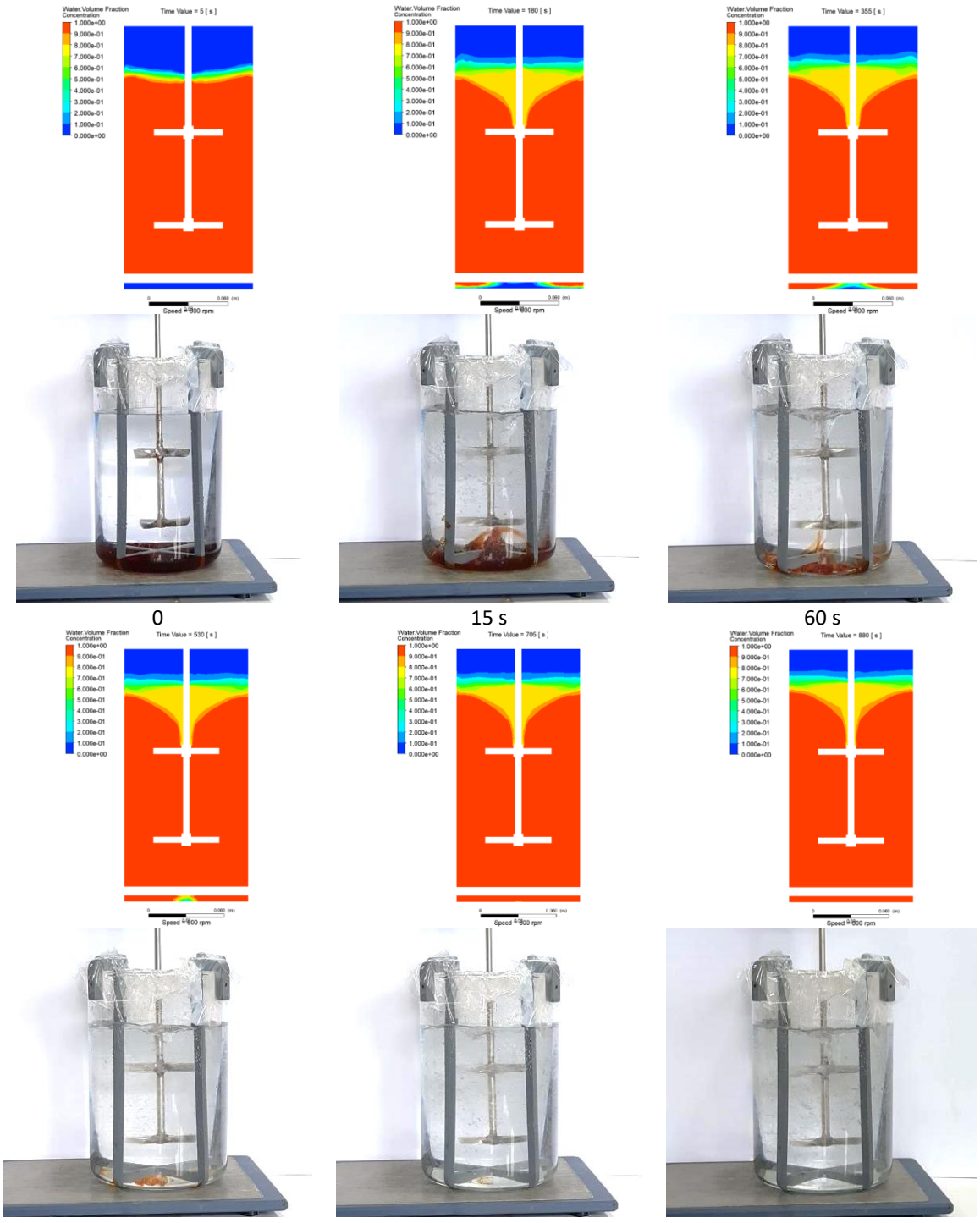

Fig. 6. Snapshots of simulated concentration contours in a 2 L baffled fermenter with 600 RPM (Top). Snapshots of red dye mixing in the 2 L baffle fermenter with 600 RPM (Bottom). Red and blue indicate high and low water volume fractions, respectively

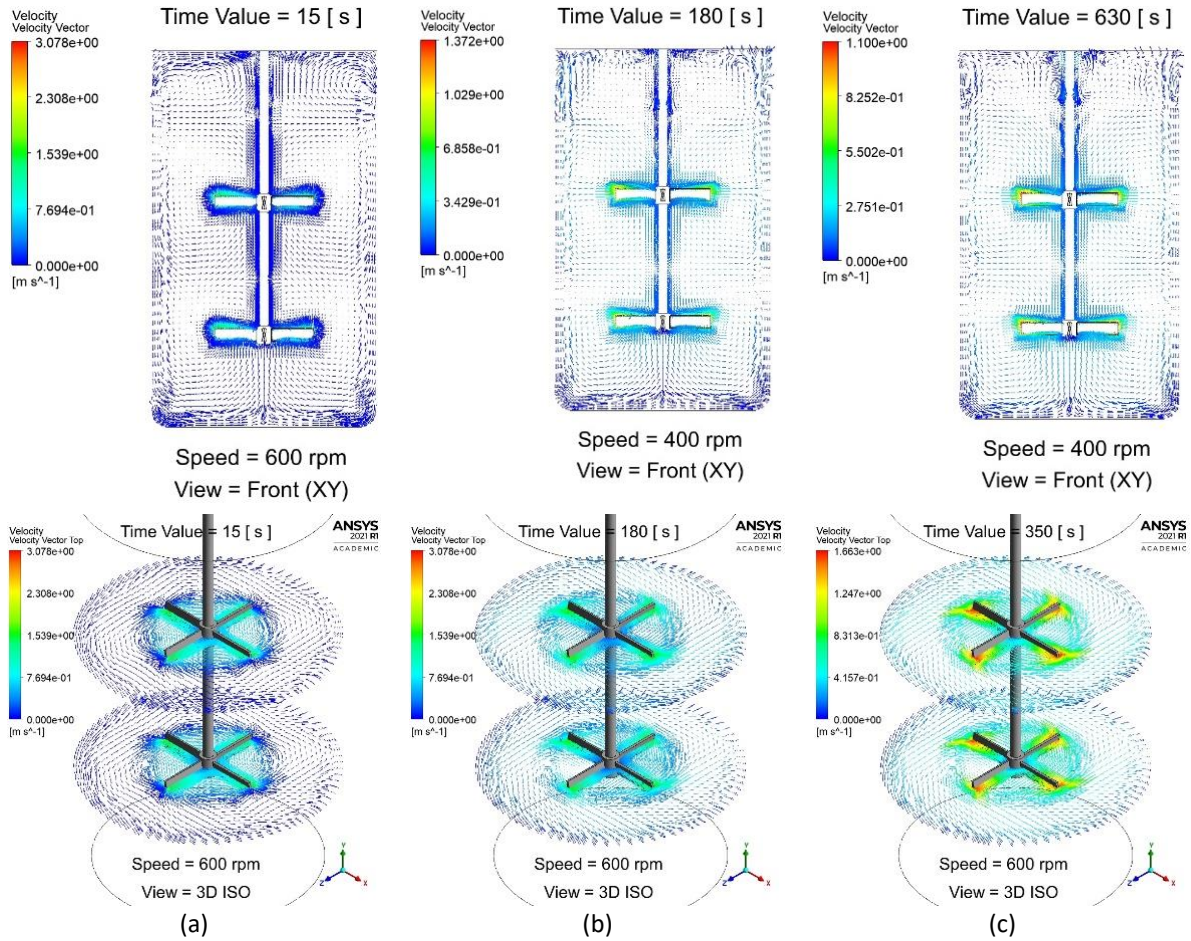

(a) (b) (c)

Fig. 7. The velocity vector of the glucose-water mixture in unbaffled fermenters at 600 RPM with mixing times: (a) 15 s, (b) 180 s, and (c) 350 s

Figure 8 depicts two circulation loops positioned above and below the impeller. As a result of the momentum change between fluid and suspended particles, the velocities closed by the upper loops are less than those in a fermenter with no baffle. The baffle fermenter could diminish these abrupt flow diversions so that there is no obvious re-circulation at the tank's base. As illustrated in Figure 8, the liquid is drawn into the propeller and expelled. Three circulation loops form beneath and above the propeller. The liquid undergoes intense mixing in circulation loops, persists to vertical flow among the draft tube and the wall, and is then forced back to the draft tube. It is important to note that the velocity profile reduces sudden flow way changes at the bottom of fermenter. Therefore, the particles-fluid interface would disrupt the symmetry and decrease the magnitude of motion loops, causing the vortices reduction and adequate mixing.

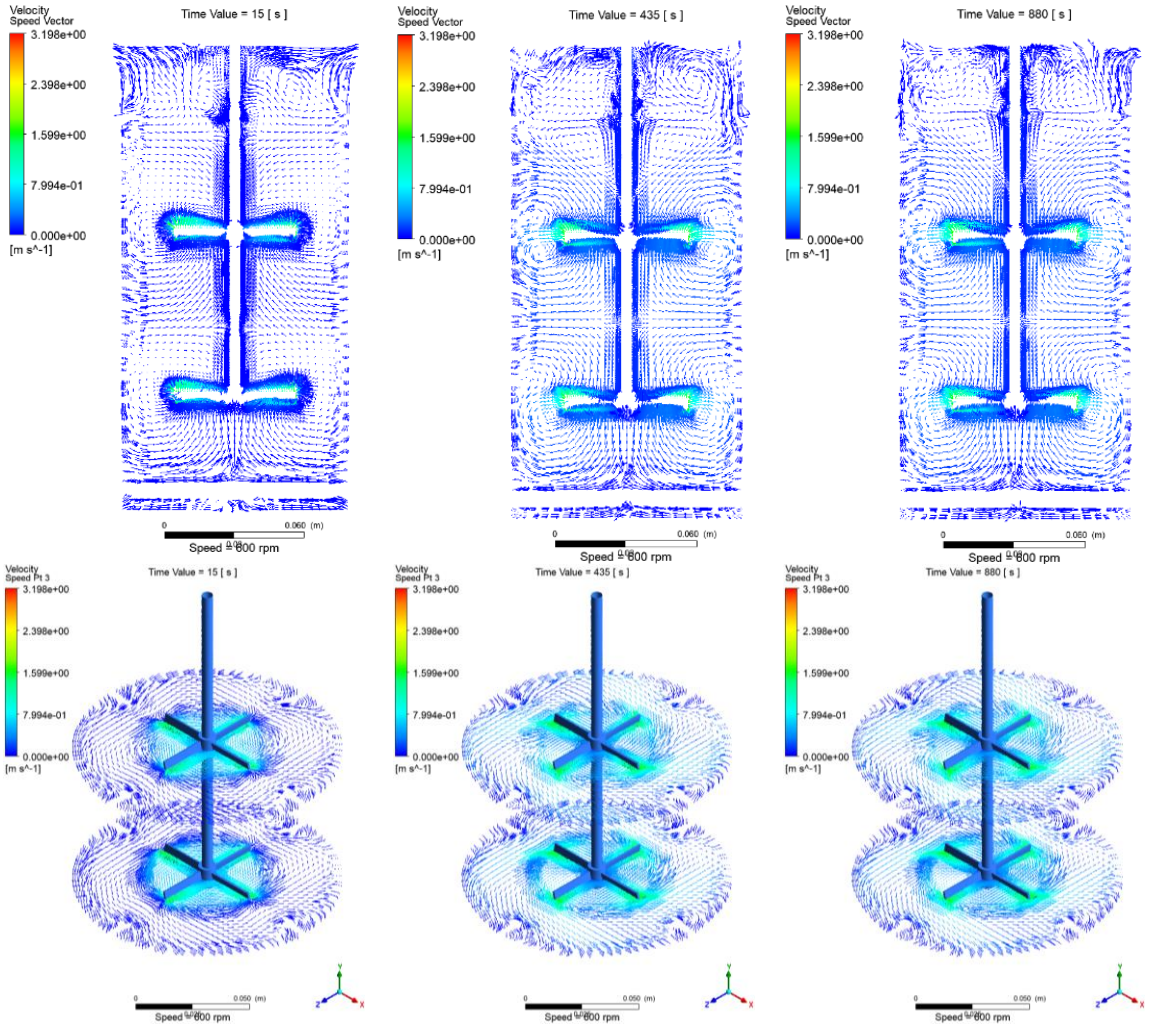

(a) (b) (c)

Fig. 8. The velocity vector of the glucose-water mixture in baffle fermenters at 600 RPM with mixing times: (a) 15 s, (b) 435 s, and (c) 880 s

Figure 9 shows the volume fraction of glucose simulated for various mixing times to determine the equivalence point of concentration, the homogeneous phase of mixing. In addition, the experimental mixing time measurement was carried out by using the coloring/decoloring process [38]. A summary of all quantitative data on mixing time on each variable can be seen in Figure 8.

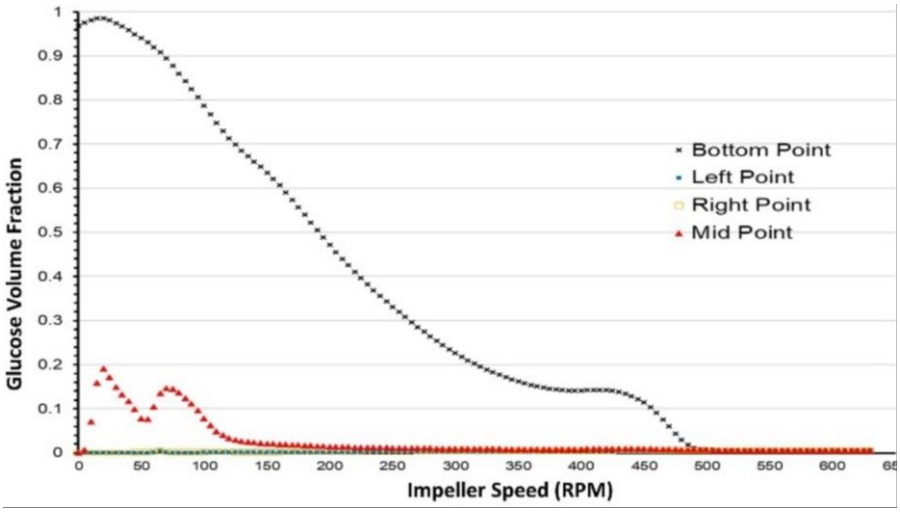
Glucose Volume Fraction
Impeller Speed (RPM)
Bottom Point
Left Point
Right Point
Mid Point

(a)

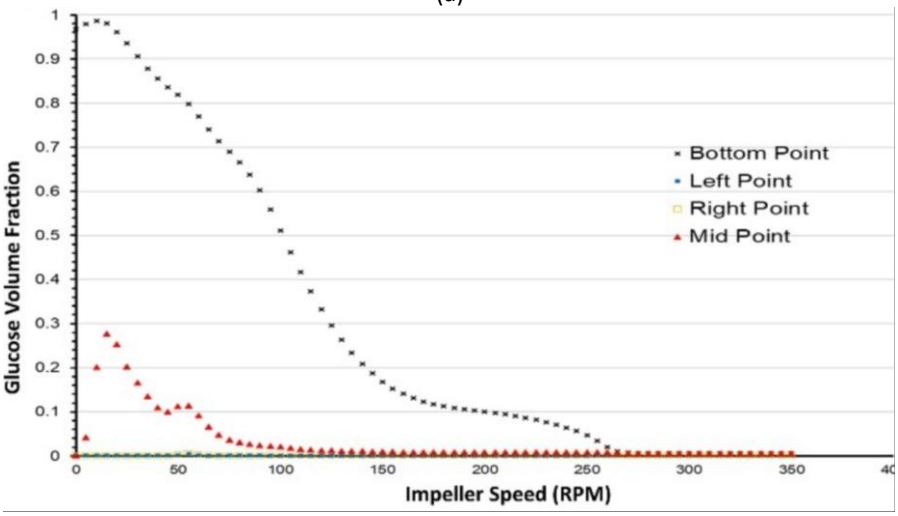
Glucose Volume Fraction
Impeller Speed (RPM)
Bottom Point
Left Point
Right Point
Mid Point

(b)

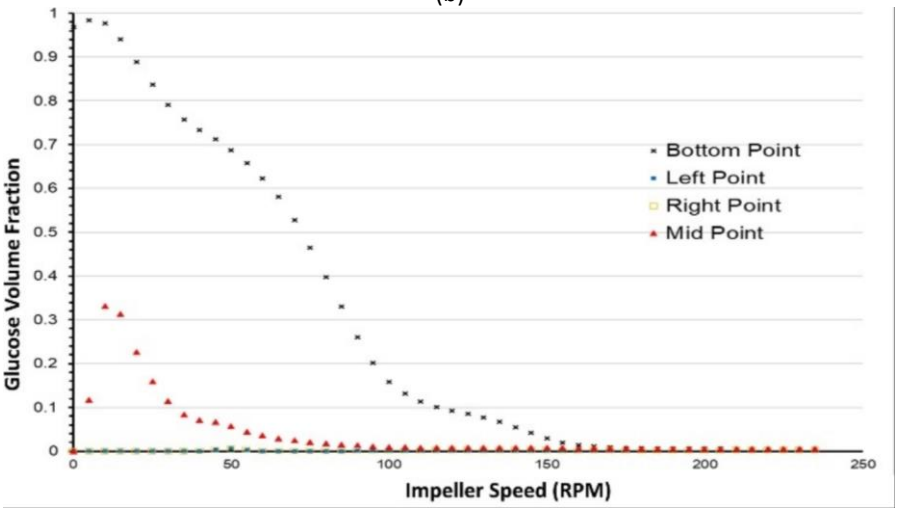
Glucose Volume Fraction
Impeller Speed (RPM)
Bottom Point
Left Point
Right Point
Mid Point

(c)

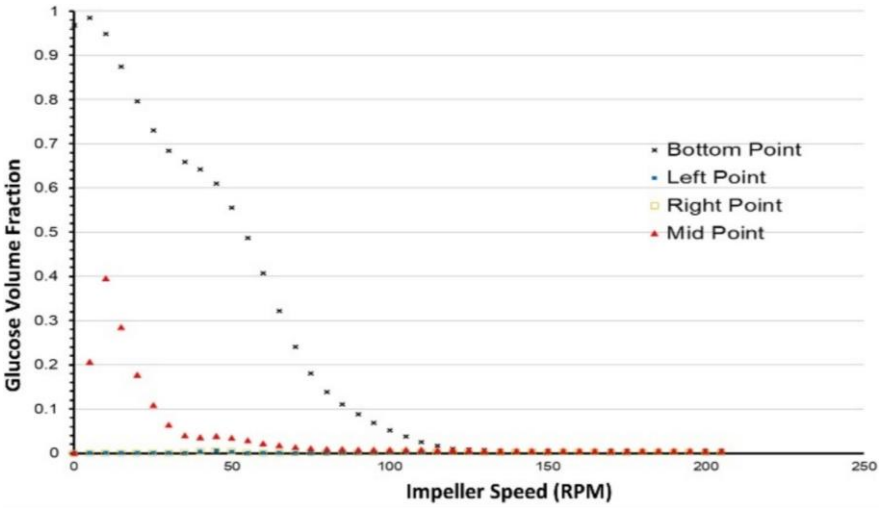
Glucose Volume Fraction
Impeller Speed (RPM)
Bottom Point
Left Point
Right Point
Mid Point

(d)

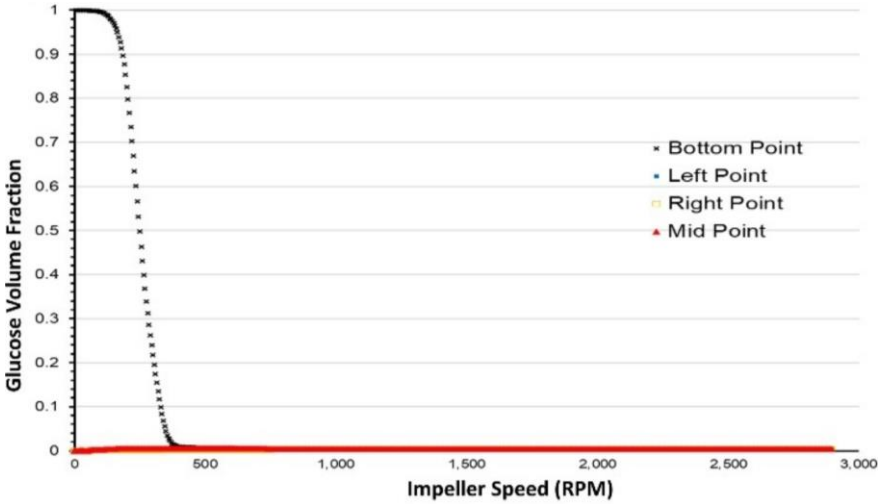
Glucose Volume Fraction
Impeller Speed (RPM)
Bottom Point
Left Point
Right Point
Mid Point

(e)

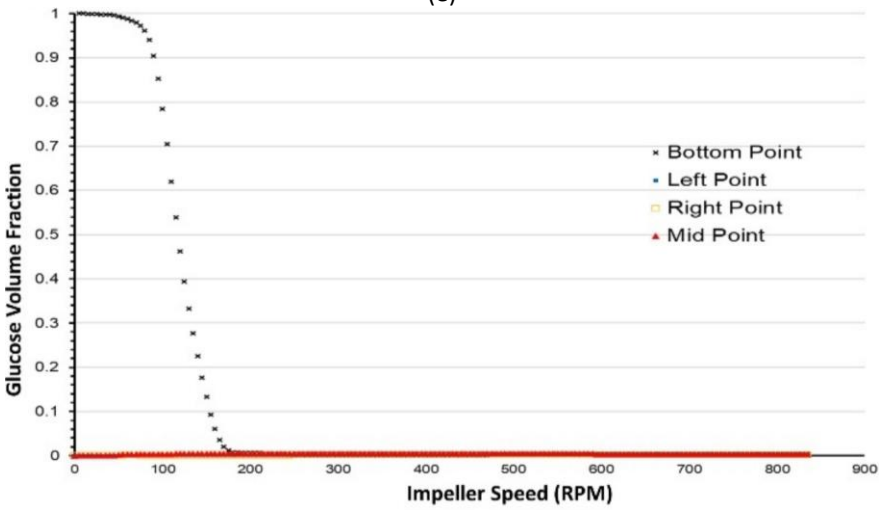
Glucose Volume Fraction
Impeller Speed (RPM)
Bottom Point
Left Point
Right Point
Mid Point

(f)

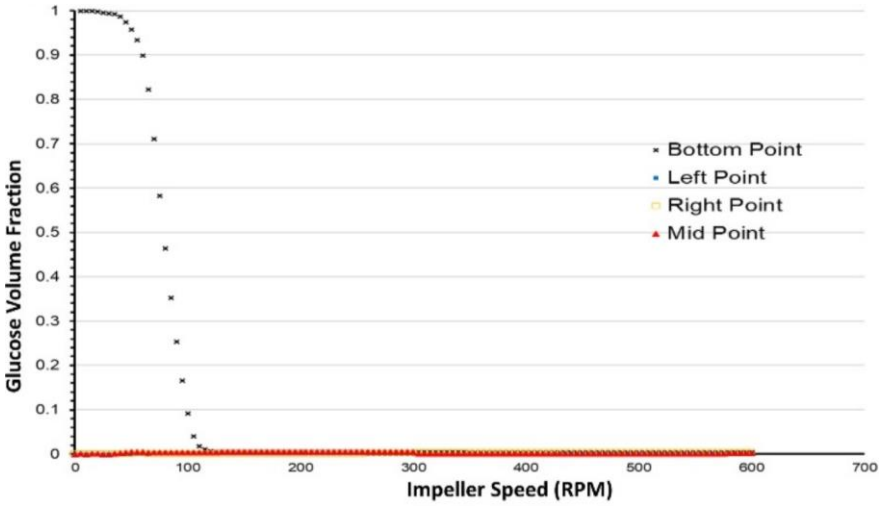

(g)

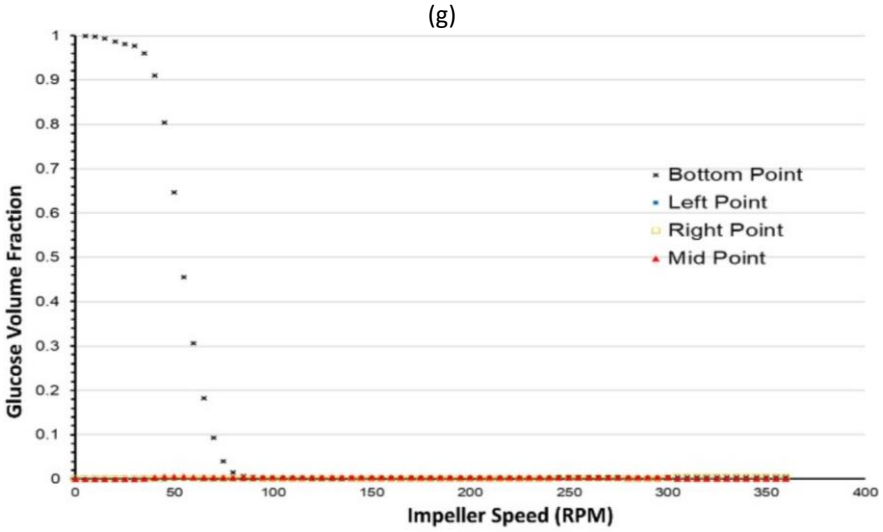

(h)

Fig. 9. The volume fraction of glucose for various mixing times at 4 points: (a) Unbaffle 400 RPM (b) Unbaffle 600 RPM (c) Unbaffle 800 RPM (d) Unbaffle 1000 RPM (e) Baffle 400 RPM (f) Baffle 600 RPM (g) Baffle 800 RPM (h) Baffle 1000 RPM

3.3 Effect of Impeller Speed on Mixing Time for Various Fermenter Configurations

From Figure 10 can be seen that the profile rate (glucose concentration against the mixing time) in most conditions tends to decrease with increasing mixing time. Since the glucose fluid has a high viscosity, glucose tends to adhere to the bottom of the tank, and the dispersion phenomenon is not constant. This phenomenon can be verified through experimental validation that has already been carried out and seen in Figure 5 and Figure 6, which display a mixing visualization. A small portion of glucose colored with iodine solution (brown) is at the bottom of the tank in the middle of the mixing process. CFD simulation of the mixing process between water and glucose in the fermenter can predict a fairly accurate mixing time with an error of about 0.16 – 0.63%. This mixing time error can be caused by several possibilities, such as glucose volume measurements between experimental against slightly different simulations, imperfect meshing at some points, and model selection multiphase and improper momentum. The simulation results successfully obtained for the mixing process in the tank with a baffle were arguably entirely satisfactory. We can see from Figure 8 that for speeds of 200 to 600 RPM, the effect of impeller speed on mixing time decreases significantly

compared to speeds of 600 to 1000 RPM, both baffle and unbaffled configurations. The mixing time profile is required to reach a homogeneous phase to the stirring speed. The existence of baffles significantly affects the amount of mixing time obtained; in this study, the use of baffles prolonged the required mixing time. Baffles can reduce mixing time by maximizing mass transfer [36]. However, if the baffle configuration, such as geometry design and dimensions, is not optimal, it can prolong the mixing time [37]. The presence of a baffle at the bottom of the fermenter with an X-like shape used in the study interferes with this process and creates a state of excessive baffling. In this study, the mixing time value of the unbaffled fermenter is faster than the baffles.

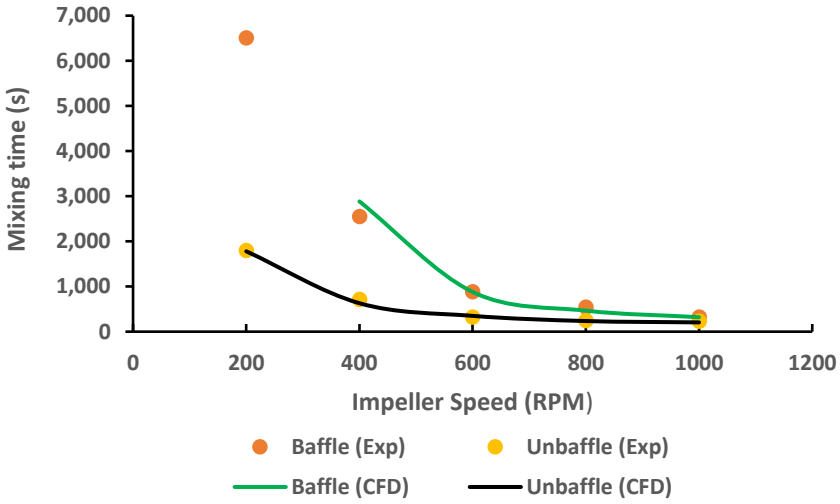

Fig. 10. Effect of impeller speed on mixing time on various variables

4. Conclusions

The effects of impeller speeds on the hydrodynamic shear stress in the unbaffled and baffle fermenter were quantified using CFD simulation. The results were validated through experiments conducted at different RPMs. Based on the results obtained from the research, it can be concluded that the condition of unbaffled fermenters is much better compared to baffle fermenters. Baffle fermenters have less shear stress and power value per time. However, they need longer mixing times. Reducing the baffle so it does not become excessive is one of the options to make the baffle fermenter more effective.

Acknowledgment
This research was not funded by any grant.

References
[1] Doran, Pauline M. "Mixing." *Bioprocess Engineering Principles* (2013): 255-332. https://doi.org/10.1016/B978-0-12-220851-5.00008-3
[2] Maluta, Francesco, Alessandro Paglianti, and Giuseppina Montante. "Towards a robust CFD modelling approach for reliable hydrodynamics and mass transfer predictions in aerobic stirred fermenters." *Biochemical Engineering Journal* 181 (2022): 108405. https://doi.org/10.1016/j.bej.2022.108405
[3] Rosa, L., L. Pederiva, G. Maurina, L. Beal, A. Torres, and M. Sousa. "CFD analysis of the effect of baffle plates on the fluid flow in an anaerobic sequencing batch reactor." *Chemical Engineering Transactions* 38 (2014): 133-138.
[4] Nadal-Rey, Gisela, Dale D. McClure, John M. Kavanagh, Benny Cassells, Sjef Cornelissen, David F. Fletcher, and Krist V. Gernaey. "Computational fluid dynamics modelling of hydrodynamics, mixing and oxygen transfer in industrial bioreactors with Newtonian broths." *Biochemical Engineering Journal* 177 (2022): 108265. https://doi.org/10.1016/j.bej.2021.108265

[5] Haringa, Cees, Robert F. Mudde, and Henk J. Noorman. "From industrial fermentor to CFD-guided downscaling: what have we learned?." *Biochemical Engineering Journal* 140 (2018): 57-71. https://doi.org/10.1016/j.bej.2018.09.001
[6] Teke, George M., Godfrey K. Gakingo, and Robert W. M. Pott. "Towards improved understanding of the hydrodynamics of a semi-partition bioreactor (SPB): A numerical investigation." *Chemical Engineering Research and Design* 177 (2022): 210-222. https://doi.org/10.1016/j.cherd.2021.10.026
[7] Kreitmayer, Diana, Srikanth R. Gopireddy, Tomomi Matsuura, Yuichi Aki, Yuta Katayama, Hirofumi Kakihara, Koichi Nonaka, Thomas Profitlich, Nora A. Urbanetz, and Eva Gutheil. "Numerical and experimental characterization of the single-use bioreactor Xcellerex™ XDR-200." *Biochemical Engineering Journal* 177 (2022): 108237. https://doi.org/10.1016/j.bej.2021.108237
[8] Vlaev, Serafim D., Iren Tsibranska, and Daniela Dzhonova-Atanasova. "Hydrodynamic characterization of dual-impeller submerged membrane bioreactor relevant to single-use bioreactor options." *Chemical Engineering Research and Design* 132 (2018): 930-941. https://doi.org/10.1016/j.cherd.2018.02.004
[9] Agarwal, Alankar, Gurveer Singh, and Akshay Prakash. "Numerical investigation of flow behavior in double-rushton turbine stirred tank bioreactor." *Materials Today: Proceedings* 43 (2021): 51-57. https://doi.org/10.1016/j.matpr.2020.11.208
[10] Duman, Emre Taylan, Ayse Kose, Yunus Celik, and Suphi S. Oncel. "Design of a horizontal-dual bladed bioreactor for low shear stress to improve hydrodynamic responses in cell cultures: A pilot study in Chlamydomonas reinhardtii." *Biochemical Engineering Journal* 169 (2021): 107970. https://doi.org/10.1016/j.bej.2021.107970
[11] Noorman, Henk J., and Joseph J. Heijnen. "Biochemical engineering's grand adventure." *Chemical Engineering Science* 170 (2017): 677-693. https://doi.org/10.1016/j.ces.2016.12.065
[12] Gao, Xi, Bo Kong, and R. Dennis Vigil. "Multiphysics simulation of algal growth in an airlift photobioreactor: effects of fluid mixing and shear stress." *Bioresource Technology* 251 (2018): 75-83. https://doi.org/10.1016/j.biortech.2017.12.014
[13] Godoy-Silva, Ruben, Jeffrey J. Chalmers, Susan A. Casnocha, Laura A. Bass, and Ningning Ma. "Physiological responses of CHO cells to repetitive hydrodynamic stress." *Biotechnology and Bioengineering* 103, no. 6 (2009): 1103-1117. https://doi.org/10.1002/bit.22339
[14] Pino, Marcela Sofía, Rosa M. Rodríguez-Jasso, Michele Michelin, Adriana C. Flores-Gallegos, Ricardo Morales-Rodriguez, José A. Teixeira, and Héctor A. Ruiz. "Bioreactor design for enzymatic hydrolysis of biomass under the biorefinery concept." *Chemical Engineering Journal* 347 (2018): 119-136. https://doi.org/10.1016/j.cej.2018.04.057
[15] Kadic, Enes, and Theodore J. Heindel. *An introduction to bioreactor hydrodynamics and gas-liquid mass transfer*. John Wiley & Sons, 2014. https://doi.org/10.1002/9781118869703
[16] Madhania, Suci, Yuswan Muharam, Sugeng Winardi, and Widodo Wahyu Purwanto. "Mechanism of molasses-water mixing behavior in bioethanol fermenter. Experiments and CFD modeling." *Energy Reports* 5 (2019): 454-461. https://doi.org/10.1016/j.egyr.2019.04.008
[17] ANSYS, I. "ANSYS FLUENT Release 2021 R1." *ANSYS, Inc., Canonsburg, PA* (2021).
[18] Rajavathsavai, Divya. "Study of Hydrodynamic and Mixing Behaviour of Continuous Stirred Tank Reactor Using CFD Tools." *PhD diss., National Institute of Technology Rourkela*, 2012.
[19] Jena, Siddharth, and Ajay Gairola. "Novel Boundary Conditions for Investigation of Environmental Wind Profile Induced due to Raised Terrains and Their Influence on Pedestrian Winds." *Journal of Advanced Research in Applied Sciences and Engineering Technology* 27, no. 1 (2022): 77-85. https://doi.org/10.37934/araset.27.1.7785
[20] Versteeg, Henk Kaarle, and Weeratunge Malalasekera. *An introduction to computational fluid dynamics: the finite volume method*. Pearson Education, 2007.
[21] Ebrahimi, Mohammadreza, Melih Tamer, Ricardo Martinez Villegas, Andrew Chiappetta, and Farhad Ein-Mozaffari. "Application of CFD to Analyze the Hydrodynamic Behaviour of a Bioreactor with a Double Impeller." *Processes* 7, no. 10 (2019): 694. https://doi.org/10.3390/pr7100694
[22] Oo, Ye Min, Makatar Wae-hayee, and Chayut Nuntadusit. "Experimental and Numerical Study on the Effect of Teardrop Dimple/Protrusion Spacing on Flow Structure and Heat Transfer Characteristics." *Journal of Advanced Research in Experimental Fluid Mechanics and Heat Transfer* 2, no. 1 (2020): 17-32.
[23] Alsadig, Ahmed, Hossin Omar, Suliman Alfarawi, and Azeldin El-sawi. "Mathematical Simulation of Baffled Shell and Tube Heat Exchanger utilizing Stream Analysis Model." *Journal of Advanced Research in Numerical Heat Transfer* 7, no. 1 (2021): 1-12.
[24] Tamburini, Alessandro, Alberto Brucato, Michele Ciofalo, Gaetano Gagliano, Giorgio Micale, and Francesca Scargiali. "CFD simulations of early-to fully-turbulent conditions in unbaffled and baffled vessels stirred by a Rushton turbine." *Chemical Engineering Research and Design* 171 (2021): 36-47. https://doi.org/10.1016/j.cherd.2021.04.021

[25] Li, Liangchao, Kefeng Xiang, and Beiping Xiang. "Numerical simulation of transient power consumption characteristics in an unbaffled stirred tank." *Chemical Papers* 74 (2020): 2849-2859. https://doi.org/10.1007/s11696-020-01115-3
[26] Davoody, Meysam, Lachlan JW Graham, Jie Wu, Peter J. Witt, Srinivasan Madapusi, and Rajarathinam Parthasarathy. "Mitigation of scale formation in unbaffled stirred tanks-experimental assessment and quantification." *Chemical Engineering Research and Design* 146 (2019): 11-21. https://doi.org/10.1016/j.cherd.2019.03.032
[27] Glover, G. M. Cartland, and J. J. Fitzpatrick. "Modelling vortex formation in an unbaffled stirred tank reactors." *Chemical Engineering Journal* 127, no. 1-3 (2007): 11-22. https://doi.org/10.1016/j.cej.2006.09.019
[28] Rotondi, Marco, Ned Grace, John Betts, Neil Bargh, Elena Costariol, Barney Zoro, Christopher J. Hewitt, Alvin W. Nienow, and Qasim A. Rafiq. "Design and development of a new ambr250® bioreactor vessel for improved cell and gene therapy applications." *Biotechnology Letters* 43 (2021): 1103-1116. https://doi.org/10.1007/s10529-021-03076-3
[29] Li, Liangchao, Jiajun Wang, Lianfang Feng, and Xueping Gu. "Computational fluid dynamics simulation of hydrodynamics in an uncovered unbaffled tank agitated by pitched blade turbines." *Korean Journal of Chemical Engineering* 34 (2017): 2811-2822. https://doi.org/10.1007/s11814-017-0208-9
[30] Conti, Fosca, Leonhard Wiedemann, Matthias Sonnleitner, Abdessamad Saidi, and Markus Goldbrunner. "Monitoring the mixing of an artificial model substrate in a scale-down laboratory digester." *Renewable Energy* 132 (2019): 351-362. https://doi.org/10.1016/j.renene.2018.08.013
[31] Kaiser, Stephan C., Sören Werner, Valentin Jossen, Katharina Blaschczok, and Dieter Eibl. "Power input measurements in stirred bioreactors at laboratory scale." *JoVE (Journal of Visualized Experiments)* 135 (2018): e56078. https://doi.org/10.3791/56078-v
[32] Ling, Samel J., Jeff Sanny, and William Moebs. *University Physics Volume 1*. OpenStax, 2016.
[33] Nienow, Alvin W. "Reactor engineering in large scale animal cell culture." *Cytotechnology* 50, no. 1-3 (2006): 9-33. https://doi.org/10.1007/s10616-006-9005-8
[34] Odeleye, A. O. O., D. T. J. Marsh, M. D. Osborne, G. J. Lye, and M. Micheletti. "On the fluid dynamics of a laboratory scale single-use stirred bioreactor." *Chemical Engineering Science* 111 (2014): 299-312. https://doi.org/10.1016/j.ces.2014.02.032
[35] Lange, Hélène, Patricia Taillandier, and Jean-Pierre Riba. "Effect of high shear stress on microbial viability." *Journal of Chemical Technology & Biotechnology: International Research in Process, Environmental & Clean Technology* 76, no. 5 (2001): 501-505. https://doi.org/10.1002/jctb.401
[36] Kang, Qianqian, Dapeng He, Na Zhao, Xin Feng, and Jingtao Wang. "Hydrodynamics in unbaffled liquid-solid stirred tanks with free surface studied by DEM-VOF method." *Chemical Engineering Journal* 386 (2020): 122846. https://doi.org/10.1016/j.cej.2019.122846
[37] Naeeni, Sepehr Khajeh, and Leila Pakzad. "Droplet size distribution and mixing hydrodynamics in a liquid-liquid stirred tank by CFD modeling." *International Journal of Multiphase Flow* 120 (2019): 103100. https://doi.org/10.1016/j.ijmultiphaseflow.2019.103100
[38] Pogal, Gail, and Richard O. Kehn. "Mixers: Don't Let Baffles Baffle You." *Chemical Processing*. January 10, 2018.